Soft Matter

PAPER

View Article Online
View Journal

Cite this: DOI: 10.1039/d4sm01252f

Computer vision for high-throughput analysis of pickering emulsions†

Kieran D. Richards, *‡ Ella Comish and Rachel C Evans *

The quanitative analysis of solid-particle stabilized emulsions, known as Pickering emulsions, is crucial for their application in food, cosmetics, and pharmaceuticals. However, size analysis of these emulsion droplets, with diameters ranging from 5 to 500 μm, is challenging due to their non-uniform spatial and polydisperse size-distribution. Here, we investigate the application of the circle-Hough transform (CHT), a well-established computer-vision technique characterised by its ability to detect circular features in noisy images, for the seldom explored quantitative assessment of droplet size from optical microscopy images. This is particularly relevant to images where emulsions are captured in a single 2D focal plane. To implement the CHT with optical images, we have developed an open-source software application (''Hough-Scan''), which incorporates a user-friendly graphical interface for ease of use, and a tiling algorithm allowing localised regions of circles to be processed in parallel and improving computational efficiency. Using Hough-Scan, we demonstrate that the CHT has superior precision, recall and accuracy for the identification of Pickering emulsion droplets and determination of their size, compared to both manual identification and established computer vision methods. Our study demonstrates that CHT implementation using Hough-Scan can significantly increase the ease of image analysis for a diverse range of Pickering emulsion systems of varying spatial and size distribution, as well as visual artefacts common to example microscopy images.

Received 25th October 2024,
Accepted 13th February 2025

DOI: 10.1039/d4sm01252f

rsc.li/soft-matter-journal

Introduction

Pickering emulsions, also known as particle-stabilised emulsions, consist of droplets stabilised by solid particles adsorbing at the interface, preventing coalescence.[1–3] The droplets may range from a few hundred nm up to a few mm in diameter and are typically spherical in shape.[1,4] Pickering emulsions have garnered attention as attractive alternatives to surfactant-stabilised systems due to their non-toxicity and high stability, finding use in cosmetics, food technology, oil recovery, and drug delivery.[4–6]

The droplet size, distribution and packing determine their suitability for different applications.[1,7] For example, droplet diameter and volume fraction affect the rheological behaviour, with higher volume fractions in oil-in-water (O/W) emulsions showing shear-thickening behaviour,[8–10] which is crucial for controlling viscosity, texture, and flow, particularly in food and cosmetics.[11,12] Reducing the droplet size enhances the oil–water interfacial area, which is pivotal in fields like biphasic catalysis as it increases potential reaction sites.[13] Droplet size also affects the loading capacity, which can determine the delivery mode (*i.e.* orally, dermally, intravenously) for pharmaceutical applications.[14,15]

However, accurate determination of the droplet size of Pickering emulsions is not trivial. If the droplets are small (<1 μm), scattering techniques such as dynamic light scattering (DLS) or small-angle X-ray-scattering (SAXS) can be used.[5,16] This is typical when emulsifying nanoparticles such as gold,[17] nano silica[18] or cellulose nanocrystals.[19] If larger particles are used (>1 μm), or the particle concentration is low, the resulting emulsion droplets are too large to be captured by these methods.[20,21] Laser diffraction techniques are capable of analysing larger droplets, but require significant sample volumes (tens of mL), usually obtained through dilution, thereby altering their morphology (*i.e.* packing/arrangement of droplets).[22,23] Diffraction techniques also use mathematical reconstruction, *e.g.* by Mie theory, where experimental errors such as multiple scattering in concentrated samples, are difficult to quantify.[24]

Microscopy is a valuable alternative to evaluate the dimensions of emulsions. For larger (>5 μm) droplets, optical microscopy, which is simple, inexpensive and requires smaller volumes (often a single drop), can be used to provide a qualitative assessment of the emulsion characteristics.[5,25]

Department of Materials Science and Metallurgy, University of Cambridge, CB3 0FS, UK. E-mail: rce26@cam.ac.uk, k.d.richards@swansea.ac.uk

† Electronic supplementary information (ESI) available: Description of emulsion compositions; (2) detailed explanation of the Hough-Scan application. See DOI: https://doi.org/10.1039/d4sm01252f

‡ Current address: Department of Chemistry, Swansea University, Swansea, SA28PP UK.

It is, however, challenging to extract meaningful quantitative data, such as mean size and distribution, from microscopy images due to factors such as overlapping droplets, varying image quality, and non-uniform droplet distributions. Conventionally, manual data extraction techniques are used to identify droplet sizes and radii.[26–30] Droplets are individually identified, by eye, and circles are drawn around them using image processing software such as ImageJ.[31] This method, however, is extremely time-consuming and prone to systematic human errors.[25,32]

Computer vision has emerged as a powerful tool for automating data extraction from complex images. Most commonly a thresholding technique, followed by a region growing (RG) method is used to identify individual circles.[33–35] Watershedding, a method where the image is divided based on 'high-relief' areas, in this case droplet edges, may also be used.[36,37] However, typical Pickering emulsions are characterised by a high density of, often overlapping, circles that are difficult to distinguish by RG methods. To address this limitation, here we apply the Circle Hough Transform (CHT), which instead transforms the image into a parameter space where circles are detected based on patterns that correspond to circular shapes. Each point in parameter space is assigned a number of 'votes' which correspond to the likelihood of finding a circle. This makes CHT less sensitive to noise and partial occlusions in images.

The CHT has previously been used in diverse fields such as red blood-cell counting[38] and motorcycle helmet detection,[39] as well as for on-line detection of surfactant-based emulsions,[24,40,41] highlighting the versatility and robustness of the technique. For example, Becker *et al.*[24] used a previously developed CHT algorithm[42] to monitor the breakup dynamics of the O/W emulsions stabilised with Tween 20 surfactant. They observed that compared to manual sizing, CHT analysis gave accurate sizing results for video frames featuring a small number of large diameter (>100 μm) droplets.

To our knowledge, CHT for quantitative assessment of the morphology of Pickering emulsions has not previously been explored. Here, we evaluate the suitability of CHT for analysing this challenging class of emulsions, which commonly form packed structures of many droplets or polydisperse structures with many overlapping droplets.[1,5,26] We have developed an open-source software application, ''Hough-Scan'',[43] which utilises the OpenCV image library,[44] and to lower the barrier of entry, includes a user-friendly interface that enables easy input of image pre-processing parameters. A tiling algorithm and parallel processing are also included to reduce the computational burden associated with analysing high-resolution images of tens to hundreds of droplets. Using the Hough-Scan application, we compare the precision, recall (the proportion of all droplets that are correctly identified) and accuracy of CHT to standard manual and RG methods for the quantitative analysis of a diverse range of Pickering emulsion systems, demonstrating its broad applicability. Our study demonstrates that CHT implementation using Hough-Scan can significantly increase the ease of image analysis for Pickering emulsions compared to existing methods.

Experimental

Materials

Fumed silica (200 nm diameter, product number: S5130), silicone oil (100 cSt, product number: 378 364, b.p. >140 °C) and mineral oil (product number: 330779, d: 0.838 g mL^{-1} at 25 °C) were purchased from Sigma Aldrich. Potato starch (product number: CHE3618, batch: 307 946, moisture $<20\%$) was purchased from Scientific Laboratory Supplies. Casein (sodium salt, product number: BS-5861E, batch: 931ZPK) was purchased from BioServ and soybean oil (product number: J61399, LOT: P20G021, d: 0.92 g mL^{-1}) was purchased from Alfa Aesar. Copper(II) phthalocyanine (95%) and nile red (99%) were purchased from Fisher Scientific. All chemicals were used as received. Azobenzene-modified silica (Azo-silica) was prepared as previously reported.[45]

Emulsion preparation

Pickering emulsions were prepared by adding solid particles (Azo-silica, copper(II) phthalocyanine, potato starch, casein or fumed silica) to equal volumes (1 mL) of H_2O (Milli-Q®) and an immiscible oil (silicone oil, mineral oil, soybean oil or diethyl adipate). Solids were added in a range of masses (1 mg to 50 mg) to produce emulsions of varying droplet size.[7,46] Full compositions for all emulsions investigated can be found in the ESI,† Section S2. Particles were initially dispersed in oil by sonicating at room temperature for 2 min using a Fisherbrand S-series sonication bath (37 kHz, 80 W) before water was added. If particles were too hydrophilic to disperse in the oil, they were first dispersed in the aqueous phase instead. Homogenisation was then carried out using a Sciquip basic homogeniser operating at 15 000 rpm for 2 min, while cooling the samples in an ice bath. Samples were contained in a vial during homogenisation (inner diameter 16.8 mm, outer diameter 18.6 mm) and the homogeniser tip placed 8 mm from the bottom of the vial. To assess the effect of dyed droplets on image analysis, nile red or methyl orange (*ca.* 0.005 mg mL^{-1}) were used to selectively stain either the aqueous or oil phase, respectively.

Optical microscopy

Pickering emulsions were characterised by optical microscopy by pipetting a droplet of the emulsion layer onto a glass slide. Images were recorded using a Canon 400D camera mounted to a Swift 350T microscope using either a $\times4$, $\times10$ or $\times40$ objective at a resolution of 5184 $\times$ 3456 pixels (pixels). The images used in analysis were chosen to capture the widest range of morphologies possible.

Manual image analysis

All images were manually analysed by sampling random coordinates for a given image and marking three points along the inner edge of the droplets at that coordinate. The radii and position of the droplets were then estimated from the three identified points. Random coordinates were sampled until fifty droplets per image were reached. While we created a custom user interface for displaying images and defining/generating

coordinates to streamline these time-consuming tasks, they can be easily completed with standard imaging software (*e.g.* ImageJ).

Artificial test images

Artificial test images were produced manually by drawing circles of a known diameter and coordinate on an 800 × 800 pixel image. Focal plane simulation was carried out by retaining an unaltered area (circular) in the centre of the image and reducing the opacity/increasing blur further from the centre. Full images and analysis results are given in the ESI,† Section S1.

Region growing analysis (RG)

Image analysis by thresholding and RG was carried out using ImageJ.[31,33] Images were globally thresholded manually so that the image was binarized into droplets and the continuous phase. The 'analyze particles' tool was then used and the ''size'' and ''circularity'' parameters manually set to best fit the droplets of a given image. The RG technique works by scanning a thresholded image (with all pixels set to either 1 or 0) for an ''island'' (a pixel set to 1, for example) where a droplet is located. The neighbouring pixels are then tested to see if they are also part of that island (1 or 0).[33] The radius of the droplet is calculated from the area, assuming that the droplet is circular.

Circle Hough transform (CHT)

Original open-source software called ''Hough-Scan'' was developed to perform the semi-automated detection of droplets using the circle Hough transform and is available on GitHub.[43] It combines tools found in the OpenCV library with a graphical user interface (GUI) that makes it easier to select the appropriate parameters for image analysis. The software also tiles the image and analyses each tile independently to reduce the computational burden of analysing images with many circular objects. The user selectable parameters are as follows: Tile Size, Tile Overlap, Blur, Minimum Distance, Canny Upper Limit, Hough-Threshold, Min Radius and Max Radius. Further discussion of these parameters can be found in the ESI,† Section S3.

Comparative evaluation of image analysis techniques

Each image analysis method used was quantitatively assessed by two metrics, precision and recall, which are defined as:[47]

$$\text{Precision} = \frac{\text{TP}}{\text{TP} + \text{FP}}$$

$$\text{Recall} = \frac{\text{TP}}{\text{TP} + \text{FN}}$$

where TP is the number of true positives, FP is the number of false positives and FN is the number of false negatives, for a given image. A true positive is where the image analysis correctly identifies a droplet. A false positive is where a droplet is identified but is not present in the image. A false negative is where a droplet is present in the image but is not correctly identified. Fig. 1 gives diagrammatic examples of TP, FP and FN cases.

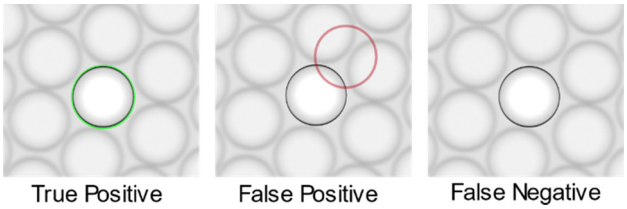

Fig. 1 Diagram showing examples of a true positive where a droplet has been correctly identified, a false positive where the circle identified does not correspond to a droplet and a false negative, where a droplet is present but is not identified.

For each image, TP and FP were determined manually. The outputs from the image analysis for a given method, *i.e.* radii and coordinates, were randomly sampled and marked as true or false by comparing them against the original image. Random sampling was achieved using the Python random module (which uses pseudo-random number generators based on the Mersenne Twister algorithm) to choose a random index of a list of droplets that had not been chosen before.

Fifty samples were taken for each image and fifty images were used in total, spanning a wide range of emulsion morphologies (compositions given in ESI,† Section S2). This sampling level provides a reasonable compromise between experimental demand (*i.e.* the time required to analyse each sample image) and a suitably robust data set for analysis.

A FN for a given image was determined by comparing a random sample of fifty manually defined droplets to the output from one of the image analysis methods and marking anything with a difference in coordinate greater than 1.5 times the radius as false (*i.e.*, coordinate ± 1.5 × radius = false). This limit was found to provide the best balance between sensitivity and specificity.

The accuracy of each method was determined by comparing the radii of fifty manually determined circles, to the equivalent circle determined by either the RG or CHT methods. For these comparisons, fifty droplets were randomly chosen in the manual image and compared to the same fifty droplets in each of the CHT/RG images. This was repeated for fifty images. It should be noted that all images were benchmarked against manual droplet identification, which as previously stated, carries its own biases due to the subjective nature of image interpretation as well as human errors. The use of these idealised measurements applies to both precision/recall metrics, as well as droplet size. A qualitative discussion is also given regarding the ease-of-use, time-to-analyse and applicability to edge cases, such as colour, contrast and resolution differences.

Results and discussion

Test images

To assess the applicability of CHT for Pickering emulsions, we first produced a series of artificial test images with known droplet sizes, which featured different common characteristics.

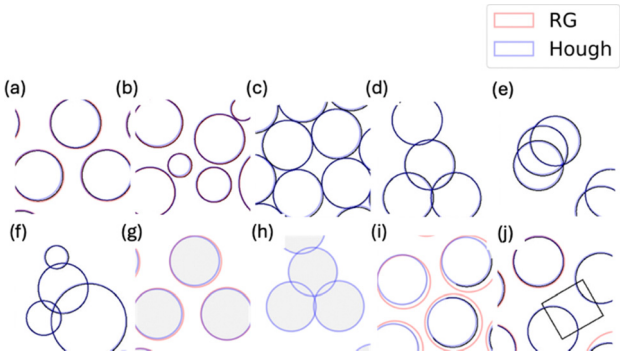

Fig. 2 Excerpts from artificially-produced test images described in ESI,† Section S1. (a)–(f) differ in polydispersity, overlap and spatial configuration. (g) and (h) are referred to as "limited contrast" emulsions and represent examples where emulsions do not appear as dark, well-defined lines. (i) shows simulation of a focal plane where droplets appear less defined toward edges of the image and (j) shows the effect of obstructive artefacts such as clumps of particle aggregate. Red lines show the position and radius of spheres identified by RG and blue lines show the spheres identified by CHT.

Fragments of each image are shown in Fig. 2 and the full images are given in ESI,† Section S1. From these images, differences in polydispersity, overlap and spatial configuration (a)–(f) can be seen, as well as variation in how the emulsion appears – either a dark line or a light grey circle (g), (h). Visual artefacts such as focal plane (i) or aggregates (shown as squares) (j) were also produced to show other common scenarios where droplet identification is difficult. In all cases the CHT excelled at identifying the artificial droplets, with 100% recall, precision and radii with 1 pixel or less difference (see ESI,† Table S1). This is also evident from inspection of Fig. 2 (blue lines) where it captures all droplets irrespective of the characteristics.

The test-images in Fig. 2 also help to highlight some of the limitations of the RG approach, as shown by the red outlines. For images where the circles are touching or overlapping, RG was unable to identify the droplets. This is because the technique has no way of differentiating one circle from another. The way that the image is thresholded prior to analysis can create either one conjoined island where circles touch, or several incomplete circles where each outline intersects. In both cases the circularity of the islands does not qualify for detection as it would compromise the accuracy in the radii. While pre-processing techniques such as watershedding may be applied, these methods need to be chosen on a per-image basis for the best results and may create new irregularities such as unintentionally splitting droplets, further compromising the accuracy of radii identification. Although not the focus of this work, these compromises can be seen in Fig. S2 (ESI†). In contrast, the CHT does not have this problem as it searches for circular objects using their edges as opposed to the islands used by RG (see ESI,† Section S3). Moreover, it can be tuned to be sensitive to incomplete circles.

For cases where droplets were successfully identified, RG showed good accuracy (less than 2 pixels different). The exception to this is Fig. 2(i) where the global threshold used causes the edges of the in-focus part of the image to bleed into the surrounding pixels, making the droplet appear bigger. This causes the droplets to be on average 4 pixels larger in size (see ESI,† Table S1).

Producing different emulsion morphologies

Having shown successful application of the CHT to artificially produced images, we now investigate real emulsion systems. Pickering emulsions can be produced in a wide range of characteristics, which vary in size, colour, polydispersity and droplet packing.[1,20,26] As such, it was important that a diverse range of emulsion systems samples were used to evaluate the broad applicability of each method. Representative optical microscopy images for the diverse sample morphologies studied are shown in Fig. 3 (see ESI,† Section S2 for sample compositions). We note that for simplicity of comparison, the image scalebars are not shown and instead emulsion droplet sizes are measured in pixels.

From inspection of Fig. 3, important morphological characteristics of Pickering emulsions can be identified. Firstly, we can see that emulsions may be highly polydisperse (a) or nearly monodisperse (b). Packing also varies from tightly packed (b), where there is little space between the droplets, to loose-packed (c), where droplets are spread out. Highly polydisperse, but tightly packed, emulsions (d) have droplets that overlap with each other making it difficult to resolve individual droplets. Emulsions may also contain coloured species (e)–(h). Nile red is

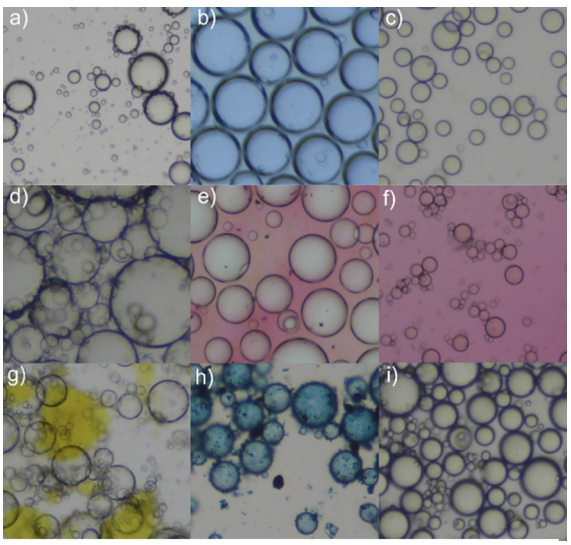

Fig. 3 Representative optical microscopy images for nine different samples, showing the diversity in appearance of different emulsions. The defining features of each image are: (a) polydisperse W/O emulsion; (b) tightly-packed primary droplets that are nearly monodisperse in a W/O emulsion; (c) loose-packed, nearly monodisperse O/W emulsion; (d) polydisperse W/O emulsion with overlapping droplets; (e) dyed continuous phase W/O emulsion; (f) dyed continuous phase W/O emulsion occluding the dispersed phase; (g) coloured particle aggregation (yellow regions) in destabilised W/O emulsion; (h) coloured particle at interface of O/W emulsion; (i) tightly-packed polydisperse W/O emulsion with dark rings around droplets.

a dye that may be used in either the continuous phase or the dispersed phase (depending on whether a water-in-oil (W/O) or O/W emulsion is produced).[48] Note that where the continuous phase is dyed and droplets are small, both phases may appear coloured as the continuous phase occludes the dispersed phase (f). We can also produce emulsions using coloured particles. Examples include Azo-silica (g), used in previous work by our group,[45] and copper(II) phthalocyanine (h), a dye which has previously been shown to stabilise Pickering emulsions.[26] In the former example, coloured particles aggregate in the oil phase forming challenging image-artefacts (g – irregular yellow shapes in background), but those at the interface of the emulsion do not produce a colour. In the latter, the particles sit at the interface and the droplets appear coloured (h – blue droplets). The addition of dyes may also affect droplet detection by either increasing (h) or decreasing (f) the contrast between the two phases. Aggregated particles may also appear similar to droplets, *i.e.*, dark, round features, which may be difficult to differentiate, depending on the technique.

Fig. 3 also shows examples of both (W/O) emulsions (a) and (O/W) emulsions (c). This leads to subtle differences in contrast between the two phases in both images, with O/W (c), in this case, having a lower contrast. Other artefacts also appear in the images, which may make droplet identification difficult. For example, droplets at the edges of the image may appear blurry (i). This is common when a small condenser aperture is used to capture images with a large depth of field. Dark rings may also arise due to diffraction patterns at the edges between liquids with a different refractive index.[49] Overall, this sample set represents a diverse range of emulsion morphologies which compare the CHT and RG methods.

Global performance of CHT and RG

The circle Hough transform was evaluated against RG in terms of its precision and recall using fifty images corresponding to a diverse range of emulsions, as shown in Fig. 4(a), where each point represents a single image. Typically, the images that had a higher recall, also had a higher precision, showing that certain conditions made the emulsions easier or more difficult to analyse by both methods. The poorer precision and recall images in both sets tend to arise from the closely-packed, polydisperse emulsions.

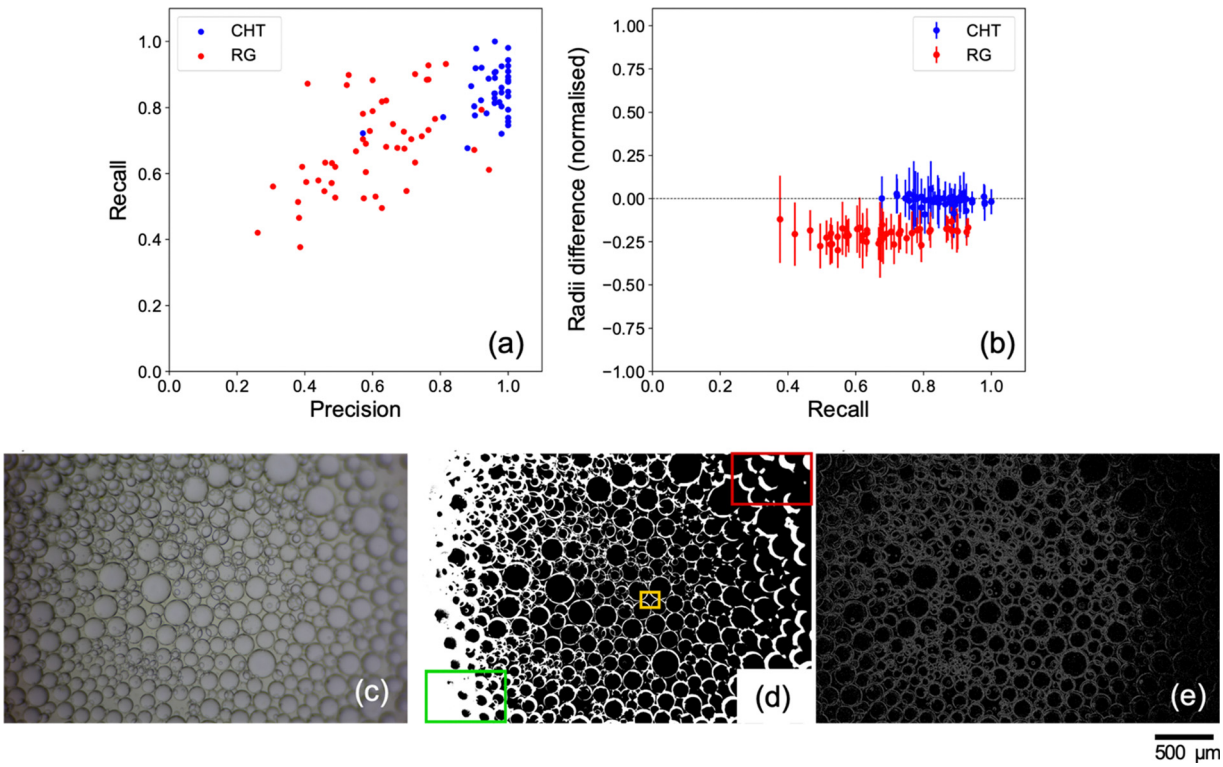

Fig. 4 Comparison in performance between the CHT and RG methods at identifying Pickering emulsion droplets from 50 images. (a) Plot of precision *vs.* recall, showing CHT has better precision and recall than RG. Images with higher precision also have higher recall, indicating that some images are easier to analyse than others. (b) Plot of recall *vs.* difference in radii between samples analysed by CHT and RG, and manually measured samples. Error bars show the standard deviation found by either method. This shows that even with better recall, CHT values for the radius are closer to the actual values, while RG underpredicts the value. The error bars show the standard deviation of the difference in radii. (c) is an example of an emulsion optical microscopy image that has been thresholded by two methods in (d) a simple threshold used in the RG and (e) a hysteresis threshold used for CHT, showing that simple thresholding has difficulty in separating the edge droplets because they out of focus in the original image. Droplet islands can merge (red rectangle, d) or not be detected (green rectangle, d) by under- and over-thresholding, respectively. The image also demonstrates how thresholding causes the droplet radii to be underpredicted as islands formed do to not extend all the way to the edges of the droplets. Also shown are false islands formed between droplets when they pack together (yellow rectangle, d). The emulsion composition can be found in the ESI,† Section S2 (Emulsion 24).

The results show that the CHT consistently outperforms the RG method. The average recall for CHT was 0.86 ± 0.08 *vs.* 0.68 ± 0.14 for RG, indicating that CHT correctly identified more circles in a given image than RG; however, neither method reached 100% droplet identification. By comparison, while 100% recall is theoretically possible by manual methods, it is extremely time-consuming (upwards of ∼40 min per image for >100 droplets) and not guaranteed due to human bias or errors due to attention span. One of the main reasons for poor recall is due to the narrow depth-of-field often seen in high-resolution microscopy images of emulsions. This is a trade-off which is usually made to capture a clear image of one layer of emulsion droplets, with the consequence that the image edge is often out of focus. CHT and RG handle out-of-focus droplets differently. RG relies on the formation of islands by thresholding. It is, however, difficult to adequately capture both the centre of the image and its edges. For instance, if the threshold is too low, islands fuse together, whereas if it is too high, they are removed altogether (Fig. 4(d)), (red and green rectangles respectively).

Workarounds exist, such as watershedding techniques, mentioned previously, and local thresholding,[33,36] but these produce other side effects such as the formation of additional islands (more false positives) or require more manual processing.[37] The CHT method, showed better recall than RG because it uses a different approach, canny edge detection (hysteresis thresholding), to segment the image (Fig. 4(e)). This method creates very thin, often discontinuous, lines around droplets. For RG, this would make droplets difficult to identify, but because CHT uses an accumulator image, complete islands are not required. CHT is still affected by out-of-focus parts of images, but to a lesser extent as a lower threshold can be used.

The mean precision, *i.e.* the fraction of all identified droplets that are correctly identified (eqn (1)), was 0.96 ± 0.07 for CHT and 0.60 ± 0.16 for RG. From Fig. 4, the precision is better for CHT than RG across all images, being close to 100% in many cases. This suggests that the RG method generates several islands that do not correspond to real droplets. Fig. 4(d) (yellow rectangle) shows that these islands occur between droplets, especially when they pack together. ImageJ uses a circularity parameter which is designed to eliminate non-spherical shapes. However, from the results here, many of these voids between droplets are spherical enough to be detected. CHT does not have the same problem as circles are not generated from islands, but instead from the edges, as mentioned previously. The voids between droplets do not produce the same bright spots on the accumulator image (see ESI,† Section S3).

When using automated analysis of droplets, there is often a trade-off between droplet identification (recall) and the accuracy of that identification. With simple thresholding and RG, for example, it is often possible to identify more islands by increasing the threshold, but those islands will be smaller than the true image (Fig. 4(d), bottom left of image). To check whether this was the case, the relationship between recall and the accuracy of radii identification was investigated. Fig. 4(b) shows the average difference in radii obtained for fifty randomly sampled droplets of fifty different images and the recall obtained for those images. Firstly, we can see that there is no significant relationship between the recall and accuracy. This suggests good technique by the operator (*i.e.*, the thresholding has been chosen to best interpret the images). The images with lower recall for RG show a greater spread in values. This suggests that the method worked well for parts of the images (the centre), and less well for other parts (the edges).

Overall, RG underpredicted the radii for all images, whereas CHT was very close to the manually identified values. The is again likely due to the specific thresholding technique used. For RG, the islands created at the centre of the droplets are smaller than the actual droplet as the boundary, which is usually quite thick, is excluded (Fig. 4(d)). This effect is compounded where dark rings appear around droplets as in Fig. 3(i). CHT does not have the same issue as it uses the edges instead of the body of the circle.

This analysis has shown that CHT works well for the case of Pickering emulsion droplets, having good precision and recall, as well as good accuracy, when compared to manual measurement. In the next section we will identify specific examples to show where CHT or RG work particularly well and any considerations that should be made when using these methods.

Performance by emulsion type

So far, we have considered all 50 images collectively, but useful information about how well each method performs can also be gained by addressing the different emulsion morphologies independently. Fig. 5 shows some representative images where poorer precision, recall and accuracy were observed.

Fig. 5(a) shows a sample containing overlapping droplets. These normally arise where there are multiple layers of small, often polydisperse, droplets, which may depend on the stability or the preparation method used to produce the emulsions.[1,9] CHT performs better here as RG cannot distinguish between two droplets that overlap and two separate droplets, as it treats any boundary as a boundary between droplets. Increased polydispersity also makes it more difficult to tune the manually input CHT and RG parameters as small droplets add less to an accumulator image in the former or do not appear as circular due to resolution constraints in the latter. This makes it more difficult to capture the different populations. Fig. 5(b) shows an emulsion which has an inhomogeneously coloured background. This occurs for unstable emulsions with coloured stabilising particles (in this case Azo-silica) which aggregate in one of the phases. RG also performs worse than CHT in this case. This is because the thresholding has difficulty separating the grey background, the yellow aggregate and the dark grey droplet edges. Instead, the yellow and dark grey regions are combined, so droplets on top of the aggregate are ignored and spaces between the aggregate and droplet edges are perceived as droplets. CHT thresholds similarly, but because the edges between the yellow and grey areas are not circular, it does not contribute significantly to the droplet identification. We note that the misidentified droplets only occur for coloured emulsions that have this inhomogeneous background. Where a more

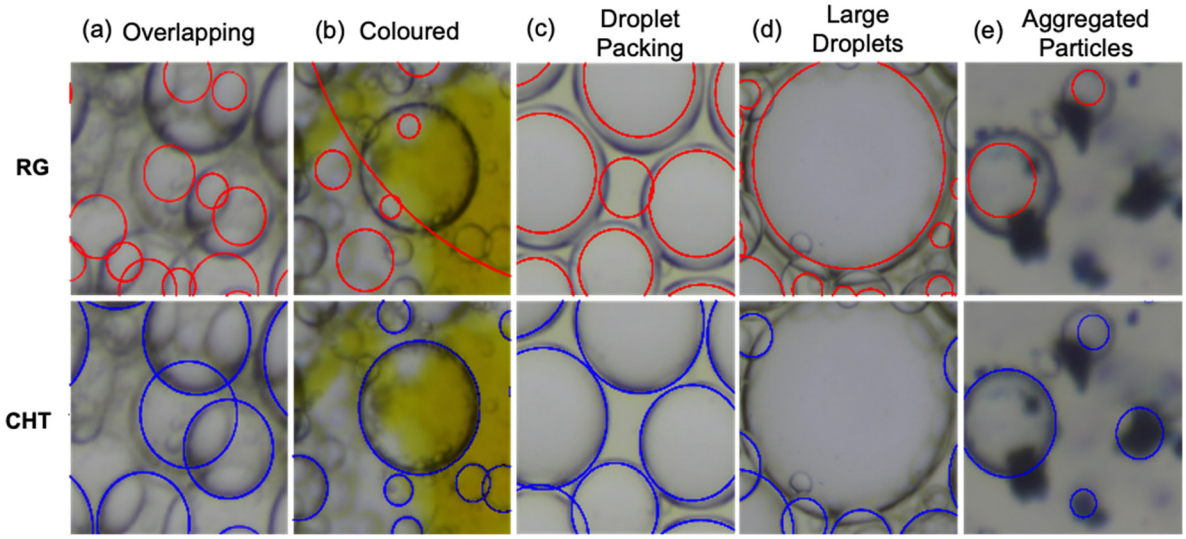

Fig. 5 Example sections taken from images with different droplet morphologies that proved challenging for identification by either the CHT or RG technique. Red and blue circles show droplet identification by RG and CHT, respectively. Image features are (a) overlapping droplets; (b) inhomogeneously coloured background caused by particle aggregation; (c) voids caused by droplet packing; (d) large droplet occupying, *ca.* 1/20th of the total image and (e) aggregated particles forming clumps in the image.

consistent colour is observed, as in Fig. 3(e), (f) and (h), the same effect was not observed.

Fig. 5(c) shows the voids that form when droplets pack together. This normally occurs for emulsions at high drop volume fractions.[50] For this case, we can see that RG interprets the void between droplets as a real droplet. This is because, when the image is thresholded, an island is formed between the droplets, which is circular enough to be recognised by RG. CHT by comparison correctly ignores the void. Fig. 5(d) shows a large droplet which is indicative of a highly-unstable emulsion. In this case, RG can identify the droplet, whereas CHT does not. This occurs when there are both very large droplets (*ca.* 1/20th of the total image) and small droplets ($<$1/100th) in the same image. Non-identification is due to the tiling algorithm used in CHT. To capture the small droplets, the tiles should be set small, but this also means that in any given tile, there is not enough of the circular interface of the large droplets to enable successful identification. Fig. 5(e) corresponds to the poorest performing image for CHT, having a precision of 0.57 (Fig. 4(a)). This arises from the presence of dark objects (aggregated particles) which form dark spots in solution which are circular enough to be interpreted as spheres at low resolution.

Challenging images and other considerations

To test the versatility of the CHT compared to RG, two artificially difficult images were produced (Fig. 6): one with low resolution, produced from an empirical image (2341 $\times$ 1640 pixels) that was artificially scaled to 0.125 its original size, and a second with the contrast reduced until droplets were barely visible by eye. Low resolution may be seen where older camera hardware is used, while low contrast is common when emulsions are made with cloudy liquids. The images were analysed by CHT and RG and the results are shown in Table 1. CHT showed good precision of 0.92 and 1.00 for the low-resolution and low-contrast images, respectively. The low-resolution image shows slightly worse precision than the high-resolution equivalent (1.00) as there are fewer pixels to add to the accumulator, and so it is more difficult to distinguish true droplets from other image artefacts. The recall was 0.96 for both images, compared to 0.94 for the unmodified image. This shows that the change in contrast or resolution does not affect the ability of CHT to correctly find droplets. The mean difference in radii was -2% (*i.e.* 2% smaller than the manually determined droplets) for both low resolution and low contrast images; this is not majorly different from the -1% of the original image.

The spread in the values, however, is significantly greater for the low-resolution sample. The unmodified image and low-contrast image had a standard deviation in the accuracy of 5 and 9%, respectively, whereas the low-resolution image is 20%. This shows that while the recall and precision are good, CHT does not accurately capture some of the low-resolution droplets. This is likely due to the poor resolution making it difficult to fit the shape of the circle accurately. By comparison, RG had a precision of 0.94 and 0.53 for the low resolution and low contrast images, respectively, compared to 0.76 for the unmodified image. The improved precision for the low-resolution image is because it is easier to distinguish droplets, with fewer visible islands produced by overlapping or close packing droplets, because of the lower detail. The recall was 0.90 and 0.73 for the low resolution and low contrast images *versus* 0.92 for the original. This is expected as, for the low contrast image, it is more difficult to separate droplets from the background when thresholding. The difference in radii was similar for both images at, *ca.* -14%, showing as mentioned previously, that thresholding erodes the edges of the droplets.

Apart from these test cases, other conditions may also arise that make image analysis challenging. For example, while Pickering emulsions typically form spheres, in unstable systems,

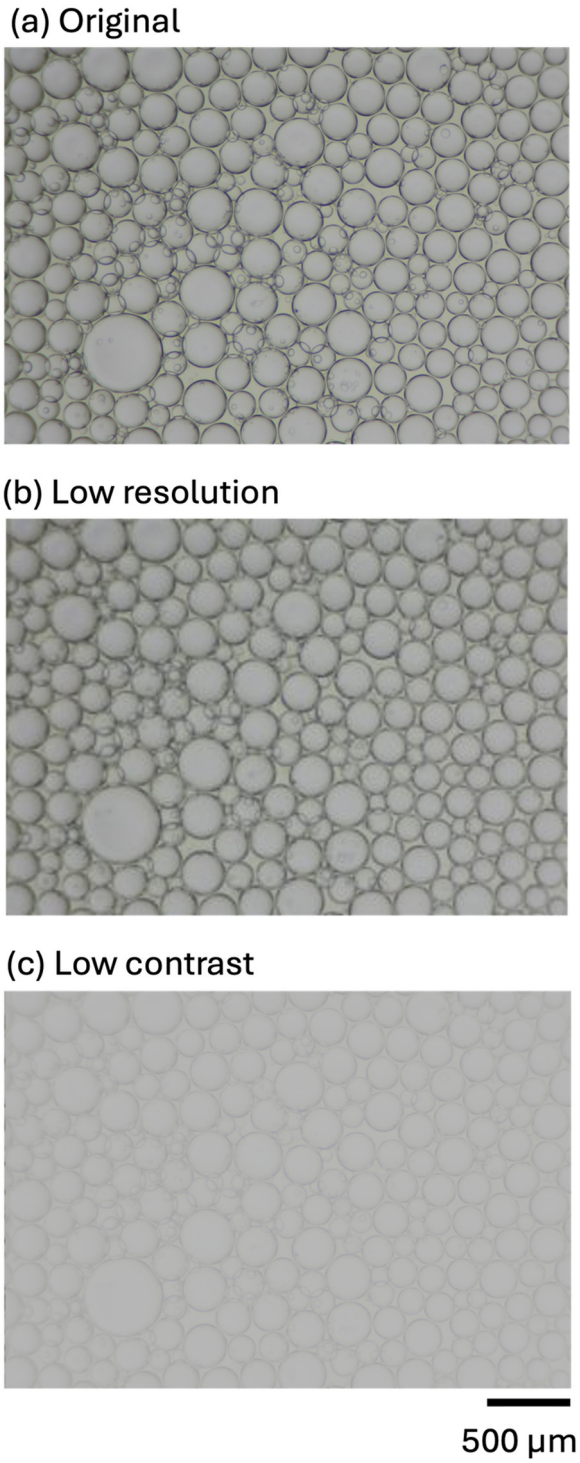

Fig. 6 Artificially-generated difficult optical microscopy images of a Pickering emulsion (Image 58, ESI,† Section S2). (a) Original image, (b) modified image with the resolution lowered from 2341 × 1640 px to 0.125 its original value (*i.e.*, 293 × 205) and (c) an image that has had its contrast artificially reduced.

processes such as arrested coalescence can occur, which may result in the formation of oblate spheroid droplets that look like two conjoined spheres.[50] These non-spherical objects are detectable by RG, but not by CHT, as they do not produce the same bright spots on the accumulator image.

Table 1 Difference in precision, recall and accuracy for the RG and CHT methods on the test image shown in Fig. 6 (Emulsion 58, ESI, Section S2), which is given in three forms – the original image, a low-resolution version and a low contrast version. The results show that the CHT method is less affected by the changes in image quality. The error in the difference in radii is given by the standard deviation

	Precision		Recall		Accuracy (%radii difference)	
Image	CHT	RG	CHT	RG	CHT	RG
Original	1.00	0.76	0.94	0.92	-1 ± 5	-20 ± 8
Low resolution	0.92	0.94	0.96	0.90	-2 ± 20	-14 ± 7
Low contrast	1.00	0.53	0.96	0.73	-2 ± 9	-15 ± 7

A final consideration is the ease of the method, which is highly dependent on the implementation. In this study, we employ the widely used ImageJ software to perform RG and compare it against the dedicated Hough-Scan tool. While ImageJ is a multi-purpose image editing tool offering many features, it does not offer purpose-built details such as a preview window to test different settings.

The run time for RG is typically <1 s and does not significantly change with the image being analysed. In contrast, CHT is more dependent on how the parameters are constrained and the image is being processed, (*i.e.*, the size, resolution and number of droplets). A well-constrained image takes <1 s (on the hardware used here, see experimental section), but images that have wide constraints (*i.e.*, a wide min. and max. range of droplets sizes) can take as long as 13 s, using the images analysed here. On balance, if analysing droplets by computer vision, where droplets are sufficiently variable that parameters need to be optimised and where high-resolution images containing densely packed droplets are used, the Hough-Scan tool is a good option in terms of usability, as it has a good balance of speed and manual refinement capabilities.

Conclusions

In summary, we have shown that CHT is a powerful computer vision tool for the quantitative assessment of Pickering emulsion droplets, outperforming the conventional RG method in terms of precision, recall and accuracy of droplet identification. The enhanced recall is attributed to the image not requiring as strong thresholding to segment droplets, and therefore capturing more of the available droplets. Better precision is, in part, due to the ability of the CHT to distinguish overlapping droplets and gaps between droplets, generating fewer false positives. CHT also showed improved accuracy, due to RG method eroding the droplet edges, leading to underprediction of the droplet radii. Moreover, CHT was able to identify droplets that could not be identified by RG, such as inhomogeneous coloured backgrounds and closely packed, overlapping droplets.

One limitation for implementation of CHT was shown – the identification of large droplets, but this can easily be overcome

by adjustments to the tiling algorithm used, *i.e.*, by performing an additional pass over the image without tiling and by constraining the possible sizes to only large droplets. We note that some of the limitations of RG can be overcome by pre-processing the image by sharpening, using deconvolution algorithms or bandpass filtering. Likewise image segmentation[33,47] including the use of watershedding, local thresholding,[33] or machine learning approaches can be used to separate droplets from the background.[51] The latter can also be used to separate layers of overlapping droplets and exclude voids which have proved challenging for RG. Similarly, pre-processing or machine-learning approaches could also be used to enhance the images that are passed to the CHT. This would likely further improve the recall and accuracy of the CHT approach, although the degree of improvement may not be as great as for RG.

In the wider context of the analysis of Pickering emulsions, we have shown that CHT provides an opportunity to work with small volumes of emulsions, which may be highly unstable, coloured or have difficult to work with images, such as those with low contrast or resolution. The process is also fast enough that there is potential to run it in real time, allowing live videos to be analysed. An exciting prospect of the CHT method is that machine learning could be used to optimise the parameters (ESI,† Section S3). This would enable completely automated droplet identification, with similar recall, precision and accuracy as the results given above. Furthermore, users could work with datasets that are too large to process manually, for example, collections of many emulsions or a single emulsion tracked *in situ* over several days. Using time-lapse photography, the CHT parameters could be self-optimised to best suit an emulsion with a changing morphology. This would also have broader implications industrially, for example in quality control, where fully-automated systems could be used to monitor emulsion composition.

Author contributions

Kieran D. Richards: conceptualisation, methodology, formal analysis, investigation, writing – original draft and visualisation. Ella Comish: formal analysis and investigation. Rachel C. Evans: supervision, project administration, funding acquisition, and writing – original draft, review and editing.

Data availability

Data for this article are available through the University of Cambridge Apollo repository at **https://doi.org/10.17863/CAM.113063**.

Conflicts of interest

There are no conflicts to declare.

Acknowledgements

K. D. R. thanks the EPSRC (EP/R513180/1) for a postgraduate studentship. We would also like to thank Kyle Richards (no affiliation) for the major contribution he made to the development of the Hough-Scan application.

Notes and references

1 C. Albert, M. Beladjine, N. Tsapis, E. Fattal, F. Agnely and N. Huang, *J. Controlled Release*, 2019, **309**, 302–332.
2 Y. Chevalier and M.-A. Bolzinger, *Colloids Surf., A*, 2013, **439**, 23–34.
3 B. P. Binks, *Curr. Opin. Colloid Interface Sci.*, 2002, **7**, 21–41.
4 D. Gonzalez Ortiz, C. Pochat-Bohatier, J. Cambedouzou, M. Bechelany and P. Miele, *Engineering*, 2020, **6**, 468–482.
5 L. E. Low, S. P. Siva, Y. K. Ho, E. S. Chan and B. T. Tey, *Adv. Colloid Interface Sci.*, 2020, **277**, 102117.
6 J. Wu and G. H. Ma, *Small*, 2016, **12**, 4633–4648.
7 J. Frelichowska, M.-A. Bolzinger and Y. Chevalier, *J. Colloid Interface Sci.*, 2010, **351**, 348–356.
8 R. Pal, *Fluids*, 2017, **3**, 2.
9 L. Hohl, S. Röhl, D. Stehl, R. von Klitzing and M. Kraume, *Chem. Ing. Tech.*, 2016, **88**, 1815–1826.
10 B. Wolf, S. Lam, M. Kirkland and W. J. Frith, *J. Rheol.*, 2007, **51**, 465–478.
11 E. Guzmán, F. Ortega and R. G. Rubio, *Cosmetics*, 2022, **9**, 68.
12 T. Xia, C. Xue and Z. Wei, *Trends Food Sci. Technol.*, 2021, **107**, 1–15.
13 M. Zhang, L. Wei, H. Chen, Z. Du, B. P. Binks and H. Yang, *J. Am. Chem. Soc.*, 2016, **138**, 10173–10183.
14 C. L. G. Harman, M. A. Patel, S. Guldin and G.-L. Davies, *Curr. Opin. Colloid Interface Sci.*, 2019, **39**, 173–189.
15 D. Marku, M. Wahlgren, M. Rayner, M. Sjöö and A. Timgren, *Int. J. Pharm.*, 2012, **428**, 1–7.
16 Y.-T. Lee, D. S. Li, J. Ilavsky, I. Kuzmenko, G.-S. Jeng, M. O'Donnell and L. D. Pozzo, *J. Colloid Interface Sci.*, 2019, **536**, 281–290.
17 K. Larson-Smith and D. C. Pozzo, *Langmuir*, 2012, **28**, 11725–11732.
18 A. Sadeghpour, F. Pirolt and O. Glatter, *Langmuir*, 2013, **29**, 6004–6012.
19 F. Cherhal, F. Cousin and I. Capron, *Biomacromolecules*, 2016, **17**, 496–502.
20 B. P. Binks and S. O. Lumsdon, *Langmuir*, 2001, **17**, 4540–4547.
21 J. Frelichowska, M.-A. Bolzinger and Y. Chevalier, *Colloids Surf., A*, 2009, **343**, 70–74.
22 E. S. Read, S. Fujii, J. I. Amalvy, D. P. Randall and S. P. Armes, *Langmuir*, 2004, **20**, 7422–7429.
23 B. P. Binks, J. Philip and J. A. Rodrigues, *Langmuir*, 2005, **21**, 3296–3302.
24 P. J. Becker, F. Puel, Y. Chevalier and N. Sheibat-Othman, *Can. J. Chem. Eng.*, 2014, **92**, 296–306.

25 D. J. McClements, *Crit. Rev. Food Sci. Nutr.*, 2007, **47**, 611–649.
26 B. P. Binks and S. O. Olusanya, *Chem. Sci.*, 2017, **8**, 708–723.
27 S. Boostani, M. Riazi, A. Marefati, M. Rayner and S. M. H. Hosseini, *Food Chem.*, 2022, **372**, 131354.
28 H. Wang, H. Du, K. Liu, H. Liu, T. Xu, S. Zhang, X. Chen, R. Zhang, H. Li, H. Xie, X. Zhang and C. Si, *Carbohydr. Polym.*, 2021, **266**, 118107.
29 T. Nallamilli, B. P. Binks, E. Mani and M. G. Basavaraj, *Langmuir*, 2015, **31**, 11200–11208.
30 Z. Rozynek, R. Bielas and A. Józefczak, *Soft Matter*, 2018, **14**, 5140–5149.
31 C. A. Schneider, W. S. Rasband and K. W. Eliceiri, *Nat. Methods*, 2012, **9**, 671–675.
32 B. Junker, *Bioprocess Biosyst. Eng.*, 2006, **29**, 185–206.
33 S. M. Hartig, *Curr. Protoc. Mol. Biol.*, 2013, **102**, 1–12.
34 E. M. Nomena and K. P. Velikov, *Colloids Surf., A*, 2019, **568**, 271–276.
35 R. Van Hooghten, V. E. Blair, A. Vananroye, A. B. Schofield, J. Vermant and J. H. J. Thijssen, *Langmuir*, 2017, **33**, 4107–4118.
36 S. Beucher, *Scanning Microsc.*, 1992, **1992**, 299–314.
37 X. Yang, H. Li and X. Zhou, *IEEE Trans. Circuits Syst. I: Regul. Pap.*, 2006, **53**, 2405–2414.
38 O. K. Bagui and J. T. Zoueu, *J. Appl. Sci.*, 2014, **14**, 3591–3594.
39 P. Doungmala and K. Klubsuwan, in 2016 IEEE International Conference on Computer and Information Technology (CIT), IEEE, 2016, pp. 611–614.
40 A. Khalil, F. Puel, Y. Chevalier, J. M. Galvan, A. Rivoire and J. P. Klein, *Chem. Eng. J.*, 2010, **165**, 946–957.
41 A. V. Patil, X. Sole Marti, P. Tetlie and S. T. Johansen, *Chem. Eng. J.*, 2017, **322**, 90–101.
42 T. Peng, A. Balijepalli, S. K. Gupta and T. LeBrun, *J. Comput. Inf. Sci. Eng.*, 2007, **7**, 330–338.
43 Hough-scan, **https://github.com/KRichardsF/Hough-Scan**, (accessed 28 May 2021).
44 OpenCV, **https://opencv.org/**, (accessed 29 September 2021).
45 K. D. Richards and R. C. Evans, *Soft Matter*, 2022, **18**, 5770–5781.
46 S. Arditty, C. P. Whitby, B. P. Binks, V. Schmitt and F. Leal-Calderon, *Eur. Phys. J. E: Soft Matter Biol. Phys.*, 2003, **11**, 273–281.
47 K. T. Mukaddem, E. J. Beard, B. Yildirim and J. M. Cole, *J. Chem. Inf. Model.*, 2020, **60**, 2492–2509.
48 R. Plenderleith, T. Swift and S. Rimmer, *RSC Adv.*, 2014, **4**, 50932–50937.
49 D. T. Grubb, *Polymer Science: A Comprehensive Reference*, Elsevier, 2012, vol. 2, pp. 465–478.
50 C. Whitby and E. Wanless, *Materials*, 2016, **9**, 626.
51 G. P. Rutkowski, I. Azizov, E. Unmann, M. Dudek and B. A. Grimes, *Mach. Learn. Appl.*, 2022, **7**, 100222.

